Appl Phys B (2010) 101: 57–63
DOI 10.1007/s00340-010-4015-9

Applied Physics B
Lasers and Optics

Blue and infrared stimulated emission from alkali vapors pumped through two-photon absorption

C.V. Sulham · G.A. Pitz · G.P. Perram

Received: 22 December 2009 / Published online: 16 April 2010

Abstract The 5 $^2D_{3/2}$, 5 $^2D_{5/2}$, and 7 $^2S_{1/2}$ states of rubidium and the 7 $^2D_{3/2}$, 7 $^2D_{5/2}$, and 9 $^2S_{1/2}$ states of cesium were populated at low pressure by two photon excitation using a pulsed dye laser. Blue beams from the Rb 6 $^2P_{3/2,\ 1/2}$–5 $^2S_{1/2}$ and Cs 7 $^2P_{3/2,\ 1/2}$–6 $^2S_{1/2}$ transitions were observed. In addition, infrared beams were observed arising directly from the pumped ^2D states, establishing a collisionless cascade mechanism. Threshold is modest at about 0.3 mJ/pulse or 2×10^5 W/cm^2. Slope efficiencies increase dramatically with alkali concentration and peak at 0.4%, with considerable opportunity for improvement. This versatile system might find applications in both underwater communications and for infrared counter measures.

1 Introduction

A new class of diode pumped lasers based on excitation of the D_2 line and subsequent lasing on the D_1 line in alkali atoms is receiving considerable attention [1]. Diode pumped alkali lasers (DPAL) have been demonstrated at 17 W with 53% slope efficiency in rubidium and 48 W (quasi-cw) with 52% efficiency in cesium [2, 3]. The lasers typically require: (1) high buffer gas pressures, ∼1 atmosphere, to match the width of the absorption profile to the spectral lineshape of the diode pump source, and (2) a collision partner such as ethane at pressures of several hundred Torr to relax the population in the pumped $^2P_{3/2}$ to the upper laser $^2P_{1/2}$. The alkali atoms provide high absorption even at low concentration and a single atom may rapidly cycle under intense pump conditions, suggesting high power operation from a small gain volume.

A similar approach has been attempted using multiple lasers to sequentially pump excited states of rubidium and cesium with the goal of lasing in the blue on the $(n+1)^2P_{3/2,\ 1/2}$–$(n)^2S_{1/2}$ transitions [4, 5]. Two, low power, cw diode lasers tuned to the D_2 line in cesium, 6 $^2S_{1/2} \rightarrow 6\ ^2P_{3/2}$ at 852 nm, and the 6 $^2P_{3/2} \rightarrow 6\ ^2D_{5/2}$ transition at 917 nm yields a ∼4 μW blue beam at 455 nm on the 7 $^2P_{3/2} \rightarrow 6\ ^2S_{1/2}$ transition [5]. Cascade through the infrared 6 $^2D_{5/2} \rightarrow 7\ ^2P_{3/2}$ at 15.1 μm presumably completes the pump cycle. Such a source might find application for laser communications through water [6]. However, the two wavelength pump requirement adds complexity to the system.

Lasing without inversion (LWI) has been demonstrated in rubidium via both a V-type and sequential double resonance processes [7–10]. In the sequential double resonance experiment, two 20 mW lasers at 780 and 776 nm produce a blue beam with power up to 40 μW by coherently coupling the 5S state with the 5P and 5D states. Detuning the 780 nm pump from the $F'' = 3 \rightarrow F' = 4$ resonance by about 2 GHz allows for higher alkali concentration and maximizes the conversion efficiency at about 0.1% [8]. A collimated infrared field at 5.5 μm arising from the 5 $^2D_{5/2} \rightarrow 6\ ^2P_{3/2}$ transition is affected only marginally by the blue beam, but the blue field occurs only when the infrared field is present [9]. Most recently, four wave mixing as the mechanism responsible for the blue light generation and the required phase matching conditions has been presented [10].

The infrared transitions are more easily inverted. Continuous-wave lasing without a resonator was demonstrated in 1981 for both Rb and Cs at 1.3–3.1 μm by pumping in the blue on the second resonances, Rb 5 $^2S_{1/2} \rightarrow 6\ ^2P_{3/2,1/2}$ and

C.V. Sulham · G.A. Pitz · G.P. Perram (✉)
Department of Engineering Physics, Air Force Institute of Technology, 2950 Hobson Way, Wright-Patterson Air Force Base, OH 45433, USA
e-mail: glen.perram@afit.edu
Fax: +1-937-6566000

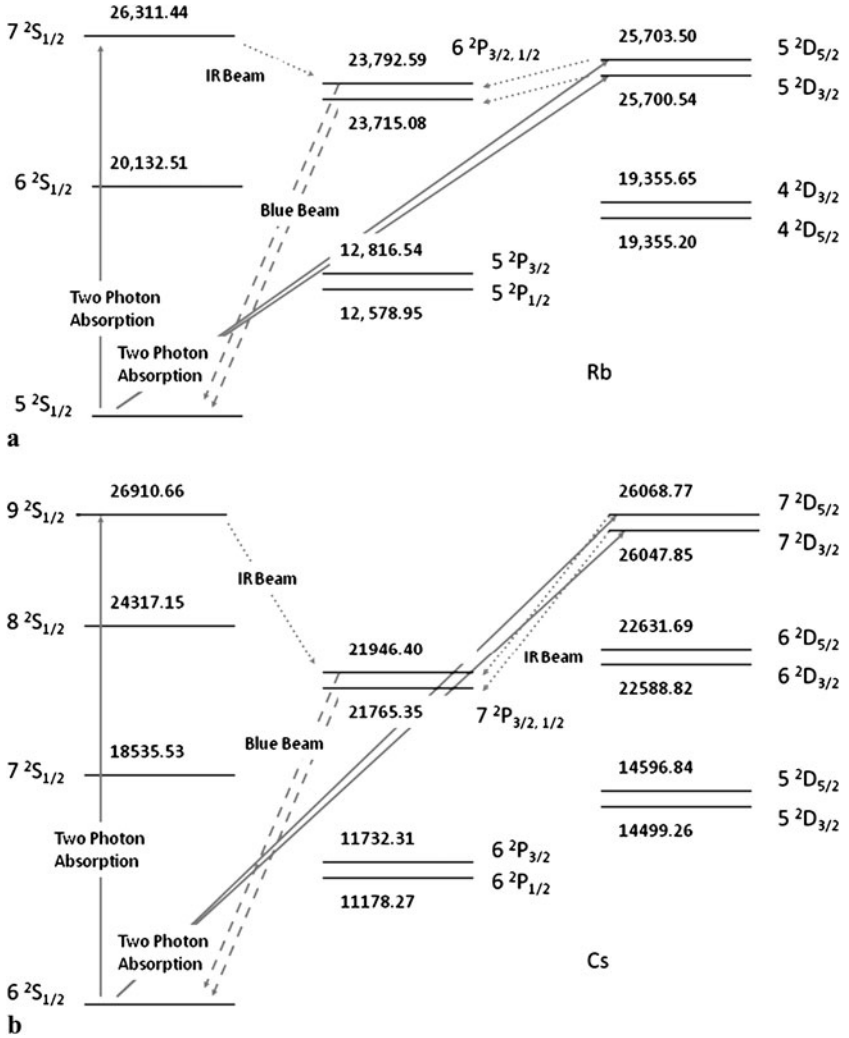

Fig. 1 Energy level diagram and lasing mechanism for (**a**) Rb and (**b**) Cs systems

Cs $6\,^2S_{1/2} \rightarrow 7\,^2P_{3/2,1/2}$ [11]. Lasing on 16 different IR lines was observed. The infrared gain-length product was about 30 and the beam divergence was about 10 mrad [11].

Another type of infrared alkali atom laser has been demonstrated based on energy transfer for optically excited alkali dimers [12, 13]. For example, broad band absorption to repulsive electronic states in the Cs_2 yields prompt dissociation and the production of the Cs $5\,^2D_{5/2,\,3/2}$ states. Lasing has been achieved at 3.01 and 3. 49 μm on the $5\,^2D_{5/2} \rightarrow 6\,^2P_{3/2}$ and $5\,^2D_{3/2} \rightarrow 6\,^2P_{1/2}$ transitions, respectively [13]. Narrow band absorption at the same pump wavelength, 584.5 nm, can produce the highly excited $9\,^2D_{5/2}$ state. Subsequent laser emission can be achieved at 2.43–8.66 μm [13]. This system requires high alkali temperatures, ∼500°C, to generate sufficient alkali dimer concentrations.

The present work generates a blue beam using a single red laser tuned to the two-photon absorption excitation of the (n) or $(n+1)\,^2D_{3/2,\,5/2}$ and $(n+2)$ or $(n+3)\,^2S_{1/2}$ states in Rb ($n = 5$) and Cs ($n = 6$), respectively. Indeed, lasing is simultaneously achieved in the mid infrared and blue after excitation in the red via the processes illustrated in Fig. 1. The system operates at low pressure without collisional energy transfer offering minimal heat load and requires only a single near infrared pump source. Conversion efficiency in the blue is similar or better than the prior double resonance experiments. Several mid infrared lasing transitions in the 2–5 μm atmospheric transmission window are also available.

2 Experimental apparatus

A schematic diagram of the laser apparatus is provided in Fig. 2. A Spectra Physics Nd:YAG pumped Sirah dye laser with LDS-765 dye, provided a tunable pump source from 745–785 nm, with up to 100 mJ in 4 ns pulses at 10 Hz and a bandwidth of ∼16 GHz. The pump beam radius of ∼3.5 mm and <0.5 mrad divergence was not a TEM_{00} mode. A 2.5 cm diameter by 7.5 cm long Triad technologies rubidium vapor cell with Pyrex windows was heated to 175–250°C in an aluminum oven. Similarly, a 2.5 cm diameter by 5.0 cm long

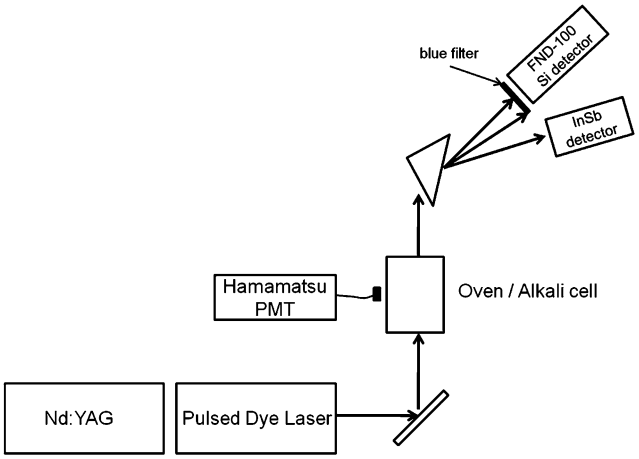

Fig. 2 Laser apparatus

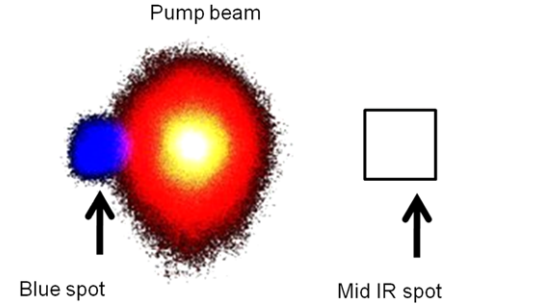

Fig. 3 Dispersed beams for the Cs cell in the forward direction. The pump beam saturates the camera. The mid IR spot was not imaged, but is schematically located by spatially scanning with the point InSb detector

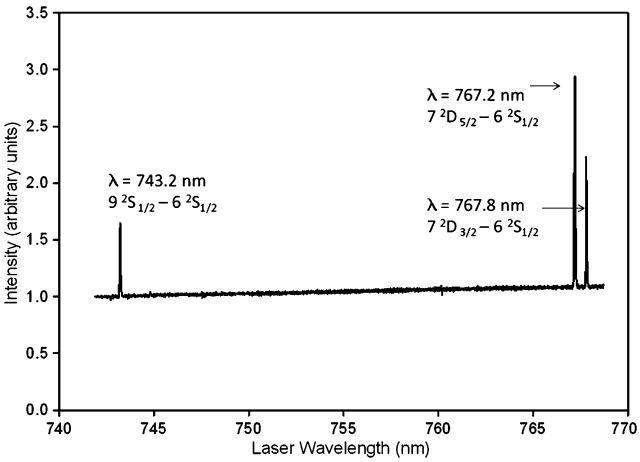

Fig. 4 Cs blue spot intensity as a function of pump laser wavelength

Triad technologies cesium vapor cell with Pyrex windows was heated to 175–200°C. Both were low pressure cells and contained no buffer gases. For rubidium, the ^{87}Rb isotope was employed, while for cesium, the natural isotopic abundance was used.

The transmitted pump and resulting stimulated beams were dispersed through a readily available BK7 prism and visually recorded with a Canon G9 CCD camera. A fast FND-100 photodiode behind a 500 nm short pass filter recorded the temporal nature of the blue beam on a 1 GHz oscilloscope. Alternatively, a large area silicon detector was employed with Boxcar detection to record laser excitation spectra. The spectral content of the blue beam was examined using a 0.5 m Triax monochromator verifying the blue ASE beams were a result of the $(n+1)^2P_{3/2,\,1/2}$–$(n)^2S_{1/2}$ transitions. Average power was measured with a Coherent LM-3 HTD or a Newport 818-SL power meter. Time resolved side fluorescence from both the blue and red ^{2}P–ground ^{2}S transitions were also monitored via a Hamamatsu R943-02 PMT. A single pixel InSb detector was employed to detect the infrared beam for the cesium laser. The cesium cell window, InSb detector response and IR filter provide an effective band pass of 2.0–2.5 μm with peak transmission of >40%, allowing for detection of the IR beam. The longer wavelengths of the rubidium system are blocked by the cell windows.

3 Results

3.1 Blue and Mid IR beam observations

A blue beam with divergence angle of $\theta_{1/2} = 6$ mrad was observed as the pump laser was tuned through the two-photon absorption wavelengths in both rubidium and cesium. A visible image of the blue beam and the transmitted far red pump laser spot recorded after the dispersing prism for the Cs cell is illustrated in Fig. 3. The blue beam divergence is larger than the pump beam, <0.5 mrad, but considerably smaller than the fluorescence solid angle of 47 mrad. A mid IR beam was also observed in Cs when the pump laser was tuned to the 7 ^{2}D$_{3/2}$–6 ^{2}P$_{1/2}$ and 7 ^{2}D$_{5/2}$–6 ^{2}P$_{3/2}$ transitions. The location and extent of the mid IR beam was determined by spatially scanning the InSb detector in the same dispersed image plane. The location of the mid IR beam is schematically overlaid on the image of Fig. 3. To ensure the IR beams were near the expected values (2.34 μm and 2.43 μm spots for the 7 ^{2}D$_{3/2}$–6 ^{2}P$_{1/2}$ and 7 ^{2}D$_{5/2}$–6 ^{2}P$_{3/2}$ transitions, respectively) a 2.5 μm long pass filter was employed and the infrared spot was no longer detected.

To validate that the alkali atoms were pumped by two-photon absorption, an excitation spectrum using the blue stimulated emission as the signal was performed. The spectrum for a cesium cell at 200°C is shown in Fig. 4. The blue spot in cesium occurred when the pump was tuned to 743.2 nm, 767.2 nm, and 767.8 nm, corresponding to the 6 ^{2}S$_{1/2}$–9 ^{2}S$_{1/2}$, 6 ^{2}S$_{1/2}$–7 ^{2}D$_{5/2}$, 6 ^{2}S$_{1/2}$–7 ^{2}D$_{3/2}$ transitions, respectively. A small leakage of the pump beam intensity through the blue band pass filter produces the observed

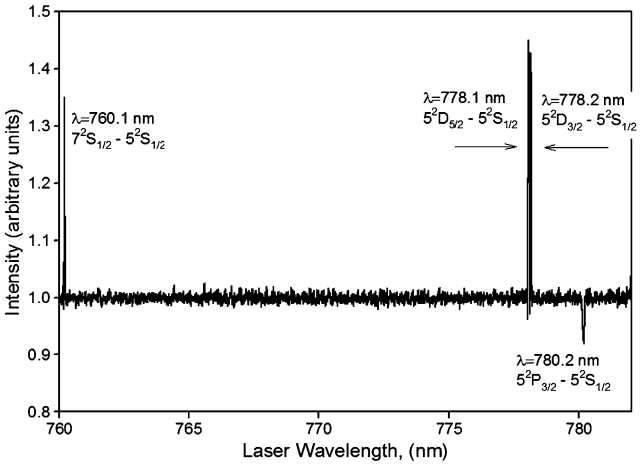

Fig. 5 Rb laser excitation spectrum for a cell at $T = 217°C$

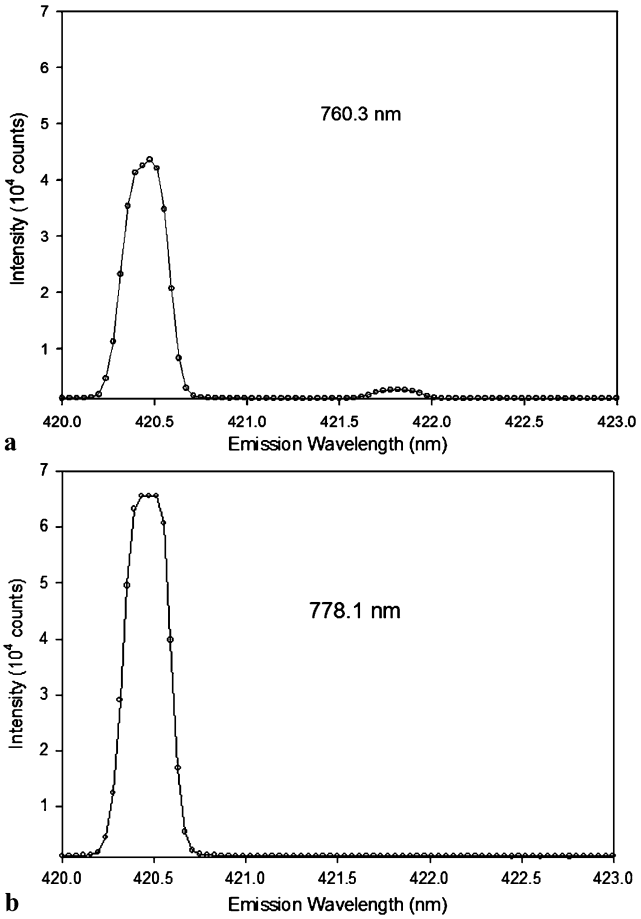

Fig. 6 Spectrally resolved blue beam intensity from the Rb cell, when pumped on the: (**a**) 5 $^2S_{1/2}$–7 $^2S_{1/2}$ line at 760.3 nm, and the (**b**) 5 $^2S_{1/2}$–5 $^2D_{3/2}$ line at 778.1 nm

baseline intensity. Similarly, the blue spots for rubidium occurred at pump wavelengths of 778.1, 778.2, and 760.1 nm as illustrated in Fig. 5. The Rb spectrum also illustrates increased absorption of the pump beam at the D_2 feature. No blue beam was observed when tuned to the D_1 or D_2 lines and the two photon lines are well outside of the wings of the D_2 absorption.

Attenuation of the pump laser at the D_2 resonance is reduced by two factors: (1) much of the pump bandwidth is outside of the absorption lineshape, and (2) the very intense pulsed laser bleaches the sample. At $T = 200°C$, the Rb concentration is $\sim 10^{15}$ atoms/cm^3 and the optical density is very high, $\sigma_{D2}[\mathrm{Rb}]\, l > 10^4$. However, the attenuation illustrated in Fig. 5 is only ~10%. The pump spectral bandwidth of 16 GHz is about 25 times larger than the unsaturated, hyperfine split, Doppler broadened D_2 line. Additional broadening or absorption in the near wings may explain additional attenuation. In Fig. 4, the pump energy per pulse is 3 mJ, providing a pump intensity of $\cong 2 \times 10^6$ W/cm^2, much higher than the saturation intensity of $I_{sat} = (h\nu/\sigma_{D2})\, A_{21} \cong 5$ W/cm^2. With a saturation parameter of $S = I/I_{sat} \cong 5 \times 10^5$, the sample is strongly bleached. At 10% absorption and 3 mJ/pulse incident, the number of absorbed photons is 1.2×10^{15}, nearly equal to the number of Rb atoms in the pumped volume. A discussion of absorption at the two photon wavelengths is provided below.

By spectrally resolving the stimulated emission for rubidium as in Fig. 6, we note that the 6 $^2P_{3/2}$–5 $^2S_{1/2}$ is 16 times more intense than the 6 $^2P_{1/2}$–5 $^2S_{1/2}$ transition when pumping the 7 $^2S_{1/2}$ state. When pumping the 5 $^2D_{3/2}$ level, lasing was limited to the 6 $^2P_{1/2}$–5 $^2S_{1/2}$ transition. When pumping the 5 $^2D_{5/2}$ level, lasing was of course limited to the 6 $^2P_{3/2}$–5 $^2S_{1/2}$ transition due to optical selection rules. Collisional relaxation between the spin-orbit split 6 $^2P_{3/2,\,1/2}$ states is minimal at these low pressures and lasing follows the strongest optical transitions between the pumped and upper laser level. Furthermore, collisional excitation of the upper laser level of the blue transition from the pumped level would be slow under the low pressure conditions. The mid IR stimulated emission appears necessary for the blue beam.

The temporal dynamics of the blue spot are illustrated in Fig. 7. The blue pulse is prompt, with minimal discernable delay of ~1 ns from the pump pulse indicating a very rapid cascade through the infrared transition. The duration of the blue beam is about 4 ns, closely following the pump pulse temporal profile. In contrast, the blue side fluorescence shown in Fig. 8 is long lived. The side fluorescence decay profile is prompt and double-exponential with an initial decay of 0.11 μs, consistent with the radiative lifetime of 0.12 μs [14]. A longer tail with decay rate of 0.53 μs is also evident. The alkali cells are optically thick and radiation trapping along the un-pumped, radial direction is clearly evident.

3.2 Threshold and slope efficiency in the blue

The energy in the blue beam pulse scales with pump energy and alkali concentration (cell temperature) as illus-

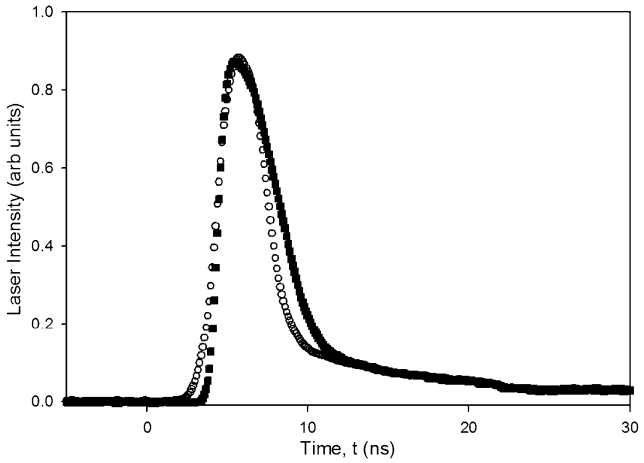

Fig. 7 Temporal profiles of the: (○) pump laser and (■) blue laser for Rb cell at $T = 175$°C pumped at 778.10 nm

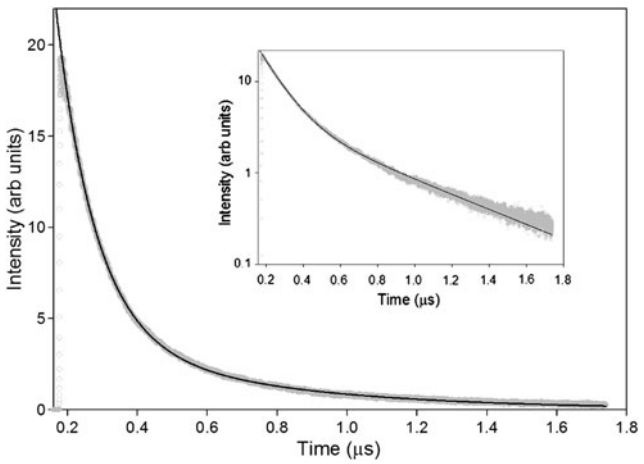

Fig. 8 Temporal profile for the side fluorescence at 420 nm for the Rb cell at $T = 175$°C pumped at 778.2 nm

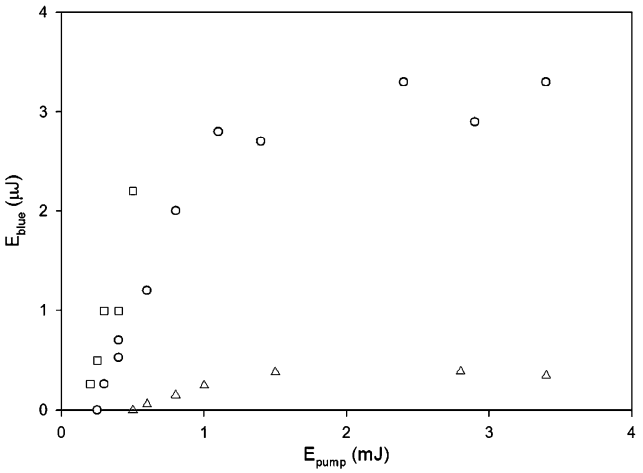

Fig. 9 Blue 6 $^2P_{3/2,\,1/2}$–5 $^2S_{1/2}$ beam energy after pulsed laser pumping of the Rb 5 $^2S_{1/2}$–5 $^2D_{5/2}$ transition at cell temperatures of: (△) 175°C, (○) 200°C and (⊡) 250°C

trated in Figs. 9–10. The blue beam exhibits a pump threshold for the Rb 5 $^2S_{1/2}$–5 $^2D_{5/2}$ transition of ∼0.3 mJ/pulse (2×10^5 W/cm^2) and somewhat higher, ∼1.5 mJ/pulse (1×10^6 W/cm^2), for the Cs 6 $^2S_{1/2}$–7 $^2D_{3/2}$ transition. Surprisingly, the threshold for Rb decreases by a factor of 2.5 as the vapor pressure increases from 0.015–.29 Torr. A similar decrease in threshold at high Cs concentration is also observed.

The blue transition slope efficiencies increase dramatically with alkali concentration, increasing from 0.03% to 0.5% for Rb as the cell temperature increases from $T = 175$ to 250°C. The peak Rb efficiency of 0.5% is about 5 times larger than reported for the previous two wavelength pump schemes [8]. The efficiency for Cs is somewhat less, 0.02–0.06% for $T = 175$ and 200°C, despite the higher vapor pressure. Almost 10 μJ per pulse or 0.1 mW average power is achieved for the scaled Cs system.

Both threshold and pump efficiency should depend on the absorption cross-section. Typically two photon absorption cross-sections are quite low. However, the cross-section for the Rb 5 $^2S_{1/2}$–5 $^2D_{5/2}$ has been calculated [15] as 0.57×10^{-18} cm^4/W and measured [16, 17] as 4×10^{-20} cm^4/W and $1.2 \pm 0.5 \times 10^{-18}$ cm^4/W. At the threshold pump energy of 0.3 mJ, the corresponding intensity is ∼200 kW/cm^2, yielding an effective absorption cross-section of 0.08–2.4 $\times 10^{-13}$ cm^2, depending on which of the prior two photon cross-sections is employed. At $T = 200$°C, the Rb concentration is 9.16×10^{14} atoms/cm^3 and the line center, unsaturated optical thickness of the two photon absorption is high, $\sigma_{2\text{photon}}[\text{Rb}]l = 93 - 2792$.

Again, the optical density is reduced by both the mismatch between the narrow absorption feature and the broad band pump, and the effects of saturation. Indeed, the 778.2 nm absorption in Rb at $T = 200$°C was observed to be about 3%. Thus, the slope efficiencies based on the number of absorbed photons is higher. At 3 mJ/pulse (2×10^6 W/cm^2) and 200°C, the Rb blue output energy per pulse is 3 μJ. For 3% of the incident photons absorbed, the blue energy corresponds to 3% of the absorbed pump energy. The addition of a buffer gas to spectrally broaden the atomic absorption feature should lead to increased absorption and slope efficiency. The output energy appears to be limited at higher pump energies particularly when the alkali concentration is low. A full description of bleaching and saturation will require a better determination of the two photon absorption cross-section and lineshapes and a thorough understanding of the kinetic processes. Finally, recall that no optical cavity was used in the present experiment. The high optical loss is probably suboptimal output coupling and efficiency may be increased with an appropriate resonator design.

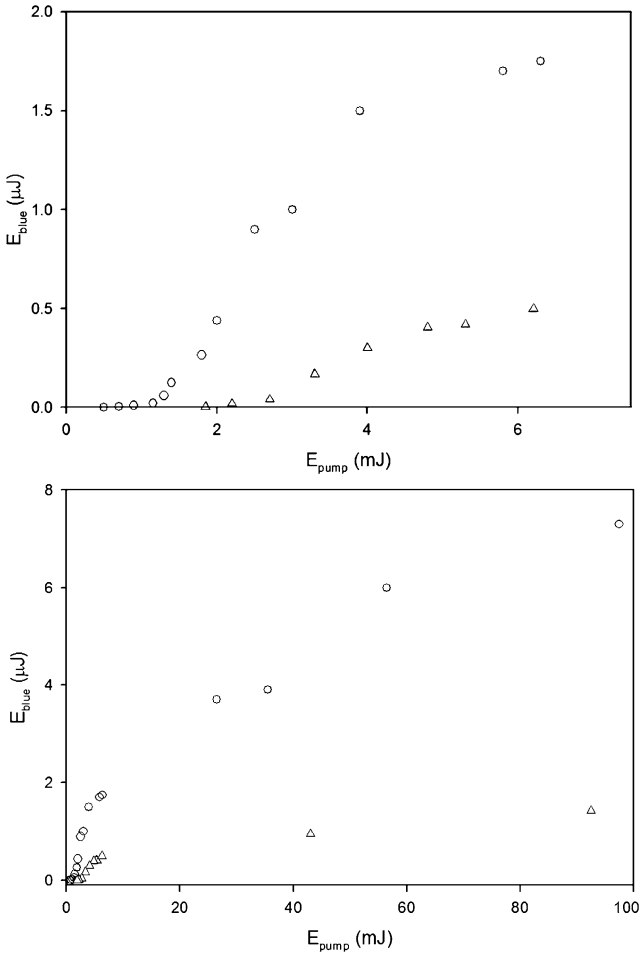

Fig. 10 Blue 6 $^2P_{3/2,\ 1/2}$–5 $^2S_{1/2}$ beam energy after pulsed laser pumping of the Cs 6 $^2S_{1/2}$–7 $^2D_{3/2}$ transition at cell temperatures of: (△) 175°C and (○) 200°C

A comparison of the blue alkali performance relative to the standard DPAL system is illustrative. The standard red DPAL typically exhibits a threshold at 4 kW/cm^2 [2, 3, 18], about 50 times less than the present results. The two photon absorption cross-section is between 2 and 60 times lower than the value for single photon absorption on the D_2 line with broadening associated with 600 Torr of helium. Thus, the relative thresholds appear consistent with the rather uncertain ratio of absorption cross-sections.

3.3 Infrared lasers

All of the current experiments were performed at low pressure with no added buffer gas and the transfer of population from the initially pumped 5 $^2D_{3/2}$, 5 $^2D_{5/2}$, and 7 $^2S_{1/2}$ states of rubidium and the 7 $^2D_{3/2}$, 7 $^2D_{5/2}$, and 9 $^2S_{1/2}$ states of cesium to the upper blue laser level $n = 6$ or 7 $^2P_{3/2,1/2}$ states occurs optically. Given the minimal delay between the pump pulse and the appearance of the blue beam as illustrated in Fig. 7, it appears that stimulated emission on the infrared

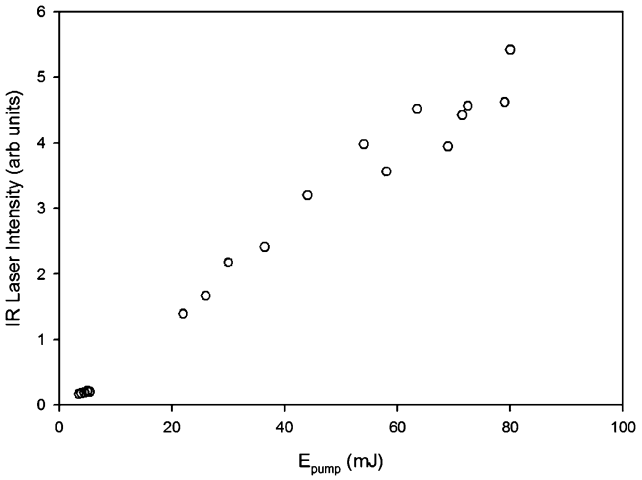

Fig. 11 Infrared beam energy after pulsed laser pumping of the Cs 6 $^2S_{1/2}$–7 $^2D_{3/2}$ transition at a cell temperature of (○) 185°C

transitions is required. Indeed, the pumped levels would immediately be inverted relative to the upper $^2P_{1/2,\ 3/2}$ levels. In cesium the wavelengths associated with these transitions range between 1.94 μm and 2.43 μm and in rubidium 3.85–5.2 μm. Using an InSb detector with two 1.5 μm long pass filters and a 2.5 μm short pass filter, the 2.34 μm and 2.43 μm spots from the 7 $^2D_{3/2}$–6 $^2P_{1/2}$ and 7 $^2D_{5/2}$–6 $^2P_{3/2}$ transitions were observed.

The intensity of the Cs infrared spot increased linearly with pump energy, with a very small threshold, as shown in Fig. 11. Since no population initially exists in the $n = 6$ or 7 $^2P_{3/2,1/2}$ states, the inversion would be prompt. The radiative lifetime of the Cs 7 $^2D_{5/2}$ state is about 88 ns [17] yielding a Doppler broadened stimulated emission cross-section of $\sigma_{IR} \cong 3 \times 10^{-10}$ cm^2. With a 100% loss per single pass, threshold is achieved at [Cs(7 $^2D_{5/2}$] $\cong 10^9$ atoms/cm^3. Assuming every absorbed photon leads to an inverted atom and 10% absorption, suggests an IR threshold pump energy of ~3 nJ/pulse (2 W/cm^2).

In contrast with the energy in the blue beam, the IR energy exhibits linear scaling with pump energy to 100 mJ. At these highest pump energies, there are more photons incident than atoms in the pumped volume. Given that the sample must be bleached at the lower threshold for the blue beams, it appears necessary that the atoms undergo a number of pump/IR/blue cycles over the short duration of the pump pulse. The transit time for a photon along the beam axis in the gain medium is about 0.2 ns and more than 10 cycles might be possible. However, the rate limiting step in the cycle would seem to be the blue transition that exhibits decreased efficiency at higher pump energies. A full interpretation of the IR and blue slope efficiencies await a thorough kinetic model of this system.

Several mid-IR laser wavelengths appear achievable under two photon pumping. In rubidium the 5 $^2D_{5/2} \rightarrow 6\ ^2P_{3/2}$

and 5 $^2D_{3/2} \rightarrow 6\ ^2P_{1/2}$ transitions at 5.03 and 5.23 μm and the 7 $^2S_{1/2} \rightarrow 6\ ^2P_{3/2,1/2}$ transitions at 3.85 and 3.97 μm are evident in the present work. Likewise, Cs operates at 2.34 and 2.43 μm for the 7 $^2D_{5/2} \rightarrow 7\ ^2P_{3/2}$ and 7 $^2D_{3/2} \rightarrow 7\ ^2P_{1/2}$ transitions and at 1.94 and 2.01 μm for the 9 $^2S_{1/2} \rightarrow 7\ ^2P_{3/2,1/2}$ transitions. Additional wavelengths of 1.87–12.14 μm may also be available by pumping the 6D and 8S states of Rb and the 8S and 6D states of Cs.

4 Conclusions

Stimulated emission on the blue ^2P–^2S transitions in Rb and Cs has been achieved by pumping at a single wavelength in the red via two photon absorption. The slope efficiency of 0.5% in Rb is considerably higher than achieved in the prior sequential double resonance experiments [8] and requires only a single wavelength pump source. Incomplete (10%) absorption of the pump photons is an important contributor to the decreased efficiency and might be improved with narrow band pumping or pressure broadening. Cascade lasing on the infrared transition followed by the blue transition offers no quantum defect and the potential for low heat loads. There would also be no need for a spin-orbit coupling gas, such as ethane, which has caused soot buildup problems in traditional DPALs cells at high temperature [19]. It appears that the performance of this system can be enhanced by scaling to higher alkali concentrations, possible in a heat pipe configuration. Threshold pump intensities are high, but the ultimate performance limits of this system have not been assessed. Indeed, a full analysis of the kinetic mechanism is required to evaluate both the scaling and efficiency of this new system. Potential applications for this new laser system include underwater communications and infrared countermeasures such as blinding heat seeking missiles.

Acknowledgements This work was funded by the High Energy Laser Joint Technology Office and Air Force Office of Scientific Research.

References

1. W. Krupke, R. Beach, V. Kanz, S. Payne, Opt. Lett. **28**, 2336 (2003)
2. B. Zhdanov, J. Sell, R. Knize, Electron. Lett. **44**, 582 (2008)
3. B. Zhdanov, A. Stooke, G. Boyadjian, A. Voci, R. Knize, Opt. Lett. **33**, 414 (2008)
4. R. Beach, W. Krupke, V. Kanz, S. Payne, Diode-pumped alkali atom lasers. UCRL-TR-210223 (2005)
5. J. Schultz, S. Abend, D. Doring, J. Debs, P. Altin, J. White, N. Robins, J. Close, Opt. Lett. **34**, 2321 (2009)
6. W. Risk, T. Gosnell, A. Nurmikko, *Compact Blue-Green Lasers* (Cambridge University Press, Cambridge, 2003)
7. A. Zibrov, M. Lukin, D. Nikonov, L. Hollberg, M. Scully, V. Velichansky, H. Robinson, Phys. Rev. Lett. **75**, 1499 (1995)
8. T. Meijer, J. White, B. Smeets, M. Jeppesen, R. Scholten, Opt. Lett. **31**, 1002 (2006)
9. A. Zibrov, M. Lukin, L. Hollberg, M. Scully, Phys. Rev. A **65**, 051801 (2002)
10. A. Akulshin, R. McLean, A. Sidorov, P. Hannaford, Opt. Exp. **17**, 22861 (2009)
11. A. Sharma, N. Bhaskar, Y. Lu, W. Happer, Appl. Phys. Lett. **39**, 209 (1981)
12. Z.-G. Wang, L.-J. Qin, L.-S. Ma, Y.-Q. Lin, I.-S. Cheng, Opt. Commun. **51**, 155 (1984)
13. M. Sitnikov, N. Znamenskii, E. Manykin, E. Petrenk, G. Grigoryan, Quantum Electron. **30**, 221 (2000)
14. C. Theodosiou, Phys. Rev. A **30**, 2881 (1984)
15. M. Marinescu, V. Florescu, A. Dalgarno, Phys. Rev. A **49**, 2714 (1993)
16. W. Zapka, M. Levenson, F. Schellenberg, A. Tam, G. Bjorklund, Opt. Lett. **8**, 27 (1982)
17. C. Collins, K. Bonin, M. Kadar-Kallen, Opt. Lett. **18**, 1754 (1993)
18. R. Beach, W. Krupke, V. Kanz, S. Payne, M. Dubinskii, L. Merkle, J. Opt. Soc. Am. B, Opt. Phys. **21**, 2151 (2004)
19. R. Page, R. Beach, V. Kanz, W. Krupke, Opt. Lett. **31**, 353 (2006)